Gas-Film Effects in the Linear Pyrolysis of Solids

R. H. CANTRELL*
Applied Physics Laboratory, The Johns Hopkins University, Silver Spring, Md.

Linear pyrolysis of solids is investigated theoretically and experimentally to determine whether gas-film effects are important. A theory to explain the effects of the gas film is developed. The theory is used with experimental data on dry ice (solid phase CO_2) to determine the magnitude of gas-film effects. It is found that there is a large temperature change across the gas film. This finding refutes the assertion of previous authors that gas-film effects are unimportant in the linear pyrolysis of solids.

Nomenclature

b = gas-film radius
c_p = specific heat at constant pressure
e = base of natural logarithms
E = activation energy
h = specific enthalpy
L = latent heat of evaporation or sublimation
m = mass flux
M = pre-exponential frequency factor in Arrhenius equation
p = pressure
q = heat flux
r = radial distance variable
R = specific gas constant
Re = Reynolds number
S = Sommerfeld number
t = function defined in Eqs. (32) and (33)
T = temperature
u = radial velocity component
w = axial velocity component
W = weight of sample, holder, and loading weight
$\mathfrak{W}$ = dimensionless weight
z = axial distance variable
λ = thermal conductivity
μ = viscosity
ξ = T/T_0 = dimensionless temperature
ρ = density

Subscripts

0 = heated surface
1 = evaporating surface
gas = gas phase
sol = solid phase
eq = thermodynamic equilibrium
∞ = ambient
s = standard or reference
av = average
max = maximum

Introduction

THE rate-controlling step in the burning of solid propellant rocket materials is believed to be the rate of surface decomposition.[1] To make laboratory determinations of this rate under simulated rocket engine conditions, Barsh et al.[2] designed a linear pyrolysis apparatus shown schematically in Fig. 1b. A propellant specimen is pressed against a heated metal surface whose temperature is comparable to that of rocket engines.

Received February 5, 1963; revision received May 20, 1963. This work is a condensation of a thesis submitted by the author to the Division of Engineering and Applied Physics, Harvard University, in partial fulfillment of the requirements for the degree of Doctor of Philosophy. This study was suggested by Howard Emmons of Harvard University. Arthur Bryson made innumerable contributions in frequent discussions with the author. Gordon Brownell of the Gordon McKay Laboratory made the experimental apparatus. The National Science Foundation gave financial support to the project.

* Physicist, Research Center. Member AIAA.

In this interpretation of linear pyrolysis data, various authors (e.g., see Ref. 3) assume no temperature change across the gas film between the heated surface and the solid's evaporating surface (solid-gas interface). This work examines that assumption theoretically and experimentally and shows that the temperature change is not always negligible.

Heat and mass transfer effects are introduced into an extended lubrication film theory. The extended theory is used to calculate evaporating surface temperature for experimental runs on dry ice (solid phase CO_2). Dry ice is used for a basic study because of its chemical simplicity.

It is customary to fit data for rate controlled (as opposed to diffusion controlled) evaporation to the Arrhenius formula

$$m = M \exp(-E/RT_1) \tag{1}$$

where m is the mass flux (g/cm²-sec), M is the pre-exponential frequency factor (g/cm²-sec), E is the activation energy (cal/mole), R is the gas constant (cal/mole °K), and T_1 is the evaporating surface temperature (°K).

Quantum and classical theories independently predict that the activation energy is equal to the latent heat of evaporation.[4] This is explicit in the reaction rate theory of Eyring (quantum) when the activated complex is assumed to be a molecule leaving the surface. It is implicit in the Knudsen equation (classical) with the aid of the Clausius-Clapeyron relation. The experimental results are in good agreement with these theories.

Comparison of the results with independent evaporation rate data for dry ice is desirable. Unfortunately, no such data have been found. Direct measurement of the evaporating surface temperature for a dry ice or propellant specimen is not feasible. The thermal boundary layer thickness in the specimen is comparable to the diameter of a thermocouple or other temperature probe.[5]

Gas-Film Theory of Linear Pyrolysis of Solids

For mathematical simplicity, the theory is developed for a gas with constant density, viscosity, and thermal conductivity. Appropriate average values for these constants are understood. The author's results[6] for a perfect gas where viscosity and thermal conductivity are functions of temperature alone are given for comparison.

In addition to the usual assumptions of lubrication film theory,[7] the assumptions of the extended theory are that energy transfer is principally due to heat conduction across the film, that the heated surface temperature is uniform, that the only chemical reaction is the solid-gas phase change, that the evaporation rate is a function of evaporating surface temperature alone, and that the solid and gas phase enthalpies are functions of temperature alone.

A solid specimen, which is forced against a constant temperature heated surface by a constant weight load, reaches a steady state rate of evaporation that is independent of radial position. The evaporating surface temperature is

therefore uniform. This implies that the heat flux

$$q = -\lambda[(T_0 - T_1)/z_1]$$

is also independent of radial position. Since q, λ, and $(T_0 - T_1)$ are independent of radial position, the film thickness z_1 is uniform.

Subject to the forementioned assumptions and preliminary conclusions, the axially symmetric steady state equations for a thin gas film are

Continuity equation

$$(1/r)(\partial/\partial r)(r\rho u) + (\partial/\partial z)(\rho w) = 0 \tag{2}$$

Momentum equations

$$\partial p/\partial r = \mu(\partial^2 u/\partial z^2) \tag{3}$$

$$\partial p/\partial z = 0 \tag{4}$$

Energy equation

$$\lambda(d^2T/dz^2) = 0 \tag{5}$$

These are four equations for the four unknowns p, T, u, and w.

The mass flux boundary conditions (see Fig. 1a) are

$$(\rho w)_{z=z_1} = -m \tag{6}$$

$$(\rho w)_{z=0} = 0 \tag{7}$$

where m is the mass flux (evaporation rate) as a function of evaporating surface temperature. The dependence of m on T_1 is immaterial in the mathematical analysis but customarily is given by the Arrhenius formula of Eq. (1).

The radial velocity vanishes on the film surfaces and on the axis of symmetry. Thus

$$u(r,0) = u(r,z_1) = u(0,z) = 0 \tag{8}$$

The pressure at the edge of the film is ambient pressure. The net force in the axial direction due to excess pressure in the film equals the weight forcing the specimen against the heated surface. Therefore, boundary conditions on the pressure are

$$p(b,z) = p_\infty \tag{9}$$

$$W = \int_0^b (p - p_\infty)2\pi r\, dr \tag{10}$$

The heat flux at the evaporating surface is given by

$$q_1 = m[h_{gas}(T_1) - h_{sol}(T_\infty)] \tag{11}$$

In practice, the bracketed quantity in Eq. (11) is calculated as a sum of three enthalpies: the enthalpy of phase change at a standard temperature, the enthalpy difference between the evaporating surface and standard temperatures for the gas, and the enthalpy difference between standard and ambient temperatures for the solid. This boundary condition replaces the energy equation for the solid.

Boundary conditions on the temperature are

$$T(r,0) = T_0 \tag{12}$$

$$T(r,z_1) = T_1 \tag{13}$$

The assumption of uniform T_0 is justified when the heated surface is a metal whose thermal conductivity is much greater than the conductivity of the gas. The uniformity of T_1 is justified by the uniform evaporation rate.

The first and second integrals of the energy equation, subject to the appropriate boundary conditions, are

$$-\lambda(dT/dz) = q = q_1 = m[h_{gas}(T_1) - h_{sol}(T_\infty)] \tag{14}$$

$$T - T_0 = -(q_1 z/\lambda) \tag{15}$$

The film thickness is then

$$z_1 = [\lambda(T_0 - T_1)/q_1] \tag{16}$$

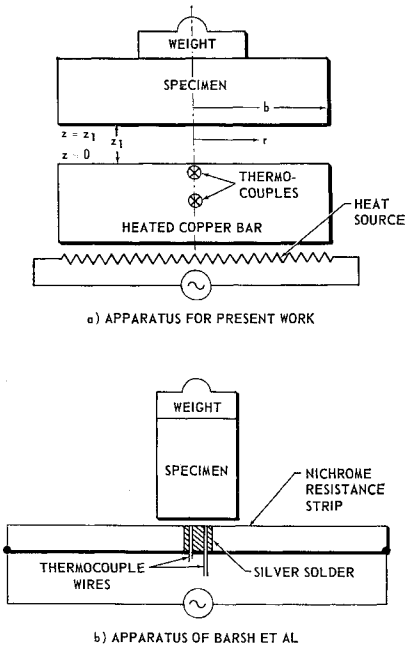

Fig. 1 Schematic drawing of linear pyrolysis apparatus

which agrees with the preliminary conclusion.

The axial momentum equation (4) implies that $p = p(r)$. The solution of the radial momentum equation subject to the boundary conditions is

$$u = \frac{dp}{dr}\frac{z(z - z_1)}{2\mu} \tag{17}$$

Since u vanishes at the axis of symmetry, $(dp/dr)_{r=0} = 0$.

Integration of the continuity equation with respect to z gives the axial velocity

$$\rho w = -\frac{\rho}{r}\frac{d}{dr}\left(r\frac{dp}{dr}\right)\left[\frac{2z^3 - 3z_1z^2}{12\mu}\right] \tag{18}$$

Evaluation of Eq. (18) at $z = z_1$ gives a differential equation for the pressure and a final expression for the axial velocity profile. They are

$$\frac{1}{r}\frac{d}{dr}\left(r\frac{dp}{dr}\right) = -\frac{12\mu m}{\rho z_1^3} \tag{19}$$

$$\rho w = m\left[\frac{2z^3 - 3z_1z^2}{z_1^3}\right] \tag{20}$$

The pressure distribution satisfying Eq. (19) and the condition $(dp/dr)_{r=b} = 0$ is

$$p = p_\infty[1 + (S/2)(1 - r^2/b^2)] \tag{21}$$

where

$$S = 6\frac{\mu[(mb/\rho z_1)/z_1^2]}{[p_\infty/b]} = \frac{6b^2\,\mu m}{p_\infty \rho z_1^3} \tag{22}$$

is a Sommerfeld number relating the viscous shear gradient to the pressure gradient. Integration of the weight loading relation Eq. (10) gives

$$W/\pi^2 b^2 p_\infty = \mathfrak{W} = S/4 \tag{23}$$

The unknown variables p, T, u, and w have been found in terms of unknown constants. Four simultaneous equations for the unknown constants T_1, m, q_1, and z_1 are

$$S = (6b^2\mu m/p_\infty \rho z_1^3) \tag{24}$$

$$m = Me^{-E/RT_1} \tag{25}$$

$$q_1 = m[h_{gas}(T_1) - h_{sol}(T_\infty)] \tag{26}$$

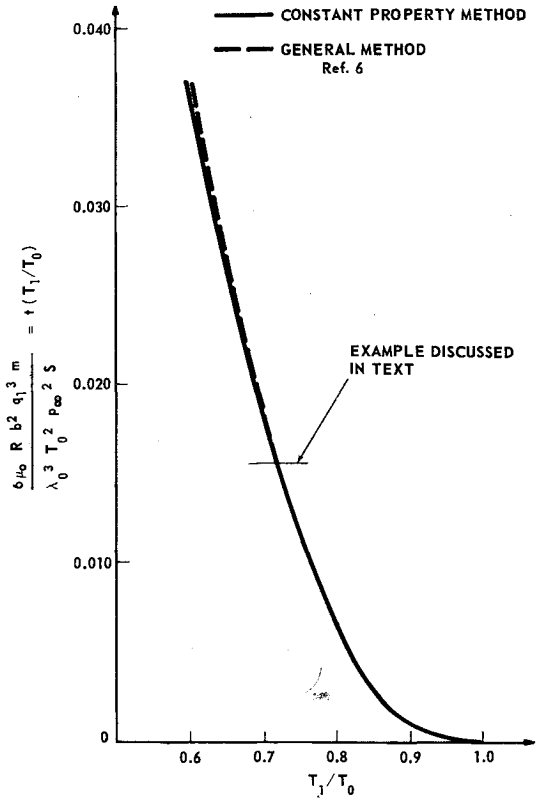

Fig. 2 Graphical solution for evaporating surface temperature of dry ice

$$z_1 = \lambda[(T_0 - T_1)/q_1] \tag{27}$$

Combination of Eqs. (24–27) gives a transcendental equation for T_1

$$\left(\frac{T_0 - T_1}{T_0}\right)^3 = \frac{6\mu b^2 M^4 e^{-4E/RT_1}}{S\lambda^3 T_0^3 p_\infty \rho} \times [h_{gas}(T_1) - h_{sol}(T_\infty)]^3 \tag{28}$$

When T_1 has been found, the remaining unknown constants are calculated easily from Eqs. (25–27).

The values of ρ, μ, and λ in Eq. [28] are understood to be appropriate values ρ_{av}, μ_{av}, and λ_{av}. A suitable value for ρ_{av} is

$$\rho_{av} = \frac{p_{av}}{R(T_0 + T_1)/2} = \frac{p_\infty(1 + S/4)}{RT_0}\left(\frac{2T_0}{T_0 + T_1}\right) \tag{29}$$

For the temperature range of interest, data from Ref. 8 show that good approximations to the thermal conductivity and viscosity of CO_2 gas are

$$\lambda/\lambda_0 = (T/T_0)^{1.5} \qquad \mu/\mu_0 = T/T_0 \tag{30}$$

Appropriate values for λ_{av} and μ_{av} are thus

$$\lambda_{av} = \left(\frac{T_0 + T_1}{2T_0}\right)^{1.5}\lambda_0 \qquad \mu_{av} = \left(\frac{T_0 + T_1}{2T_0}\right)\mu_0 \tag{31}$$

For the evaporation of dry ice in a linear pyrolysis apparatus, the transcendental equation for T_1 with transport properties evaluated at heated surface temperature T_0 is

$$t\left(\frac{T_1}{T_0}\right) = \left(\frac{T_0 - T_1}{T_0}\right)^3\left(\frac{T_0 + T_1}{2T_0}\right)^{2.5} = \frac{6}{S[1 + (S/4)]}\frac{\mu_0 Rb^2 M^4 e^{-4E/RT_1}}{\lambda_0^3 T_0^2 p_\infty^2} \times [h_{gas}(T_1) - h_{sol}(T_\infty)]^3 \tag{32}$$

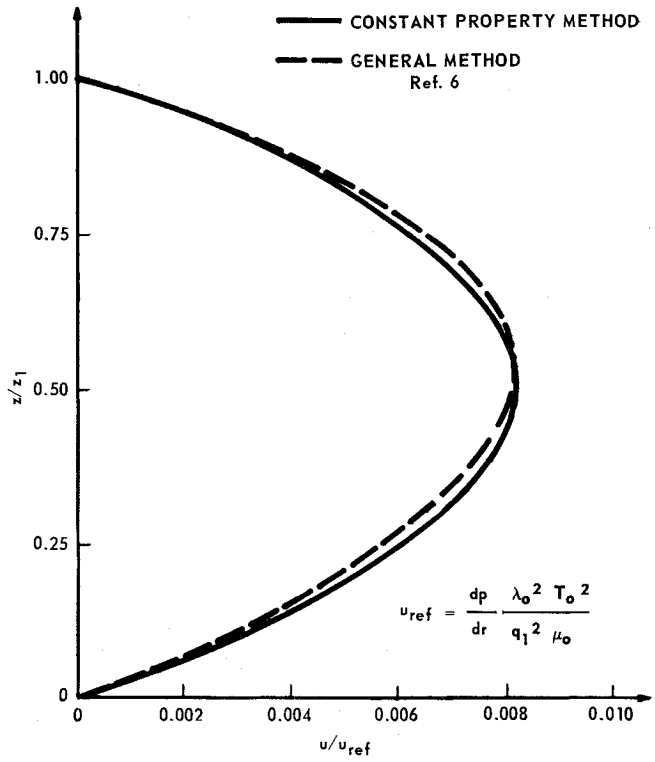

Fig. 3 Gas-film radial velocity profile for linear pyrolysis of dry ice

For a perfect gas whose viscosity and thermal conductivity are given by Eq. (30), the author[6] has obtained

$$t\left(\frac{T_1}{T_0}\right) = \frac{5 - 11(T_1/T_0)^{1.5} + 11(T_1/T_0)^4 - 5(T_1/T_0)^{5.5}}{27.5} = \frac{6}{S}\frac{\mu_0 Rb^2 M^4 e^{-4E/RT_1}}{\lambda_0^3 T_0^2 p_\infty^2} \times [h_{gas}(T_1) - h_{sol}(T_\infty)]^3 \tag{33}$$

The Sommerfeld number for the compressible flow case (perfect gas) is given implicitly by

$$\mathfrak{W} = \frac{(1 + S)^{3/2} - 1}{\frac{3}{2}S} - 1 \tag{34}$$

When S is sufficiently small so that terms of order S^2 may be neglected, this expression reduces to Eq. (23).

The results of the present analysis and the more general analysis differ by the two expressions for $t(T_1/T_0)$ on the left-hand sides and by the weight dependent factors $[6/S(1 + S/4)]$ and

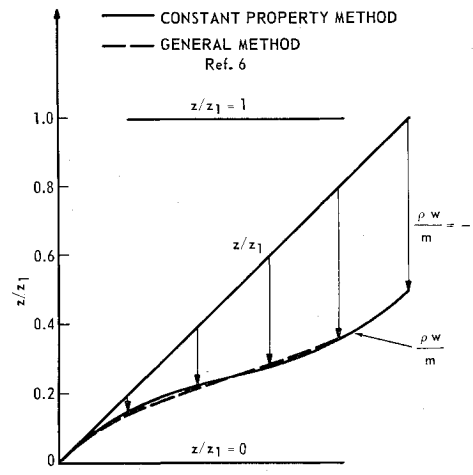

Fig. 4 Axial component of mass flux

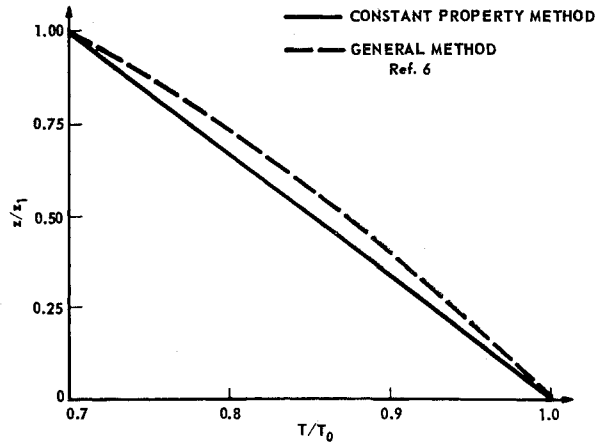

Fig. 5 Gas-film temperature distribution for linear pyrolysis of dry ice

[6/S] on the right-hand sides of Eqs. (32) and (33). The two functions $t(T_1/T_0)$ are seen in Fig. 2 to be almost identical. For small values of S, the two analyses give almost identical results. Experimental data discussed in subsequent sections are processed by the more general method since the factor $S/4$ is not always negligible. For agreement with the more general results, the factor $(1 + S/4)$ is omitted in subsequent equations. Further, it is understood that S is determined from Eq. (34). The velocity, temperature, and pressure distributions obtained by the two analyses are compared in Figs. 3–6. The differences are quite small except for the pressure distribution with large $\mathcal{W}$.

Use of the Theory to Determine Material Properties

Calculation of T_1 in terms of known properties of the solid and gas serves no useful purpose at the present time. Graphical determination of M and E in log$m$ vs $1/T_1$ coordinates is the present goal of a series of pyrolysis experiments.

To determine T_1 when M and E are unknown, one must measure one or both of the quantities m and q in addition to p_∞, T_0, W, and b. When only one of the quantities m or q

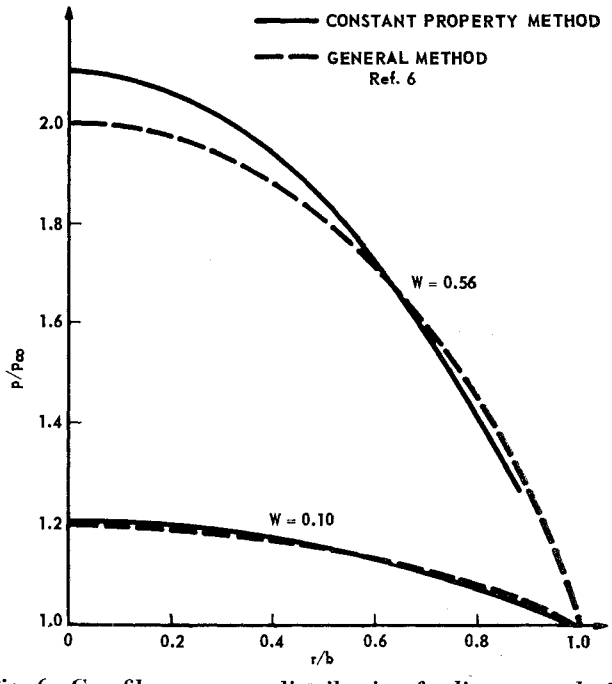

Fig. 6 Gas-film pressure distribution for linear pyrolysis

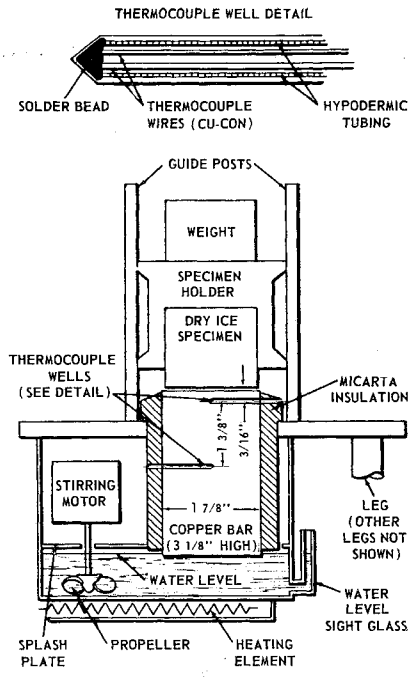

Fig. 7 Cross-section drawing of experimental apparatus

is measured, one must measure $(T_\infty)_{sol}$ and know the enthalpies associated with evaporation.

Evaporating surface temperature T_1 is obtained from

$$t\left(\frac{T_1}{T_0}\right) = \frac{6}{S}\frac{\mu_0 Rb^2 mq^3}{\lambda_0^3 T_0^2 p_\infty^2} \tag{35}$$

when both m and q are measured; from

$$t\left(\frac{T_1}{T_0}\right) = \frac{6}{S}\frac{\mu_0 Rb^2 m^4}{\lambda_0^3 T_0^2 p_\infty^2}\,[h_{gas}(T_1) - h_{sol}(T_\infty)]^3 \tag{36}$$

when only m is measured; and from

$$t\left(\frac{T_1}{T_0}\right) = \frac{6}{S}\frac{\mu_0 Rb^2}{\lambda_0^3 T_0^2 p_\infty^2}\frac{q^4}{[h_{gas}(T_1) - h_{sol}(T_\infty)]} \tag{37}$$

when only q is measured.

In the experimental work on dry ice, q was measured, but m was not. Measurement of m would have required additional equipment to determine the density of each dry ice sample. Equation (37) is therefore appropriate for the experimental phase of this work.

In an experimental apparatus, the heat flux $q = q_0$ is measured at the heated surface. According to the theory $q_0 = q_1$. This is correct to the order of the Reynolds number (when the Prandtl number is of order unity). The difference between q_0 and q_1 is shown below to be independent of position. Since terms of the order of the Reynolds number are neglected, either q_0 or q_1 may be correctly used in Eq. (37). The value q_1 is believed better because it is the value of the heat flux where the most significant heat transfer occurs.

The energy equation with convection terms included is†

$$\lambda\frac{d^2T}{dz^2} = \rho w\, c_p\frac{dT}{dz} = m(h_0 - h_1)\left(\frac{2z^3 - 3z_1z^2}{z_1^4}\right) \tag{38}$$

Integration gives

$$q_1 - q_0 = -\tfrac{1}{2}m(h_0 - h_1) \tag{39}$$

† The steady state energy equation in the form

$$\rho\mathbf{u}\cdot\nabla h = \cdot\mathbf{u}\nabla p + \Phi_{viscous} + \lambda\nabla^2 T$$

contains three terms of order Re. They are $\rho w(dh/dz)$, $u(dp/dr)$, and $\mu(\partial^2 u/\partial z^2)$. The last two terms have no net effect in the present calculation.

Substitution of Eq. (39) into Eq. (37) gives

$$t\frac{T_1}{T_0} = \frac{6}{S}\frac{\mu_0 R b^2}{\lambda_0^3 T_0^2 p_\infty^2}\frac{[q_0 - \frac{1}{2}m(h_0 - h_1)]^4}{[h_{gas}(T_1) - h_{sol}(T_\infty)]} \tag{40}$$

Equation (40) is solved in iterative form to obtain $\xi_1 = T_1/T_0$ for experimental runs. The mass flux m is calculated from Eq. (11) when q_1 and T_1 have been determined.

Experimental Apparatus and Results

A cross-section drawing of the experimental apparatus is shown in Fig. 7. The heat source in the apparatus is an agitated water bath in contact with the insulated copper bar.

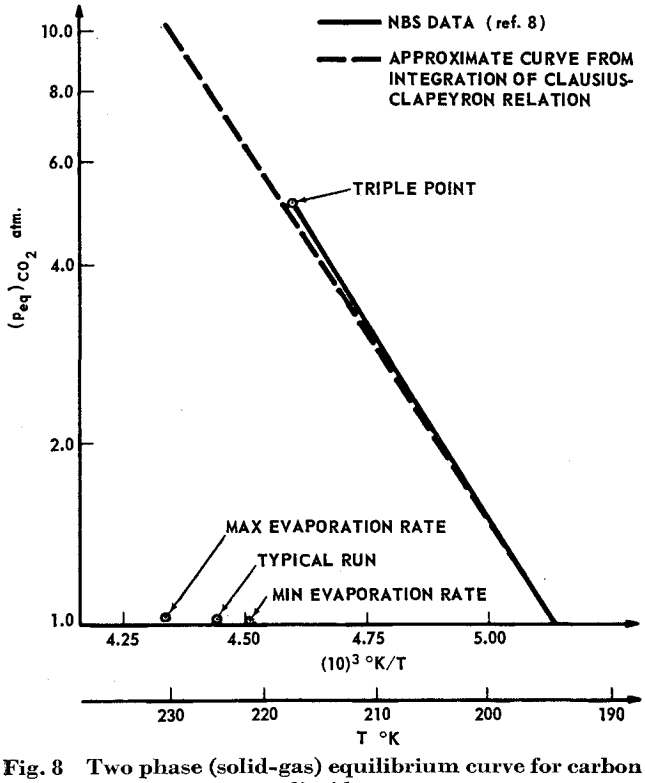

Fig. 8 Two phase (solid-gas) equilibrium curve for carbon dioxide

The construction of the holder and guide posts prevents the constant tone sound emitted by a piece of loosely held dry ice against a metal surface. No noise is heard when the dry ice specimen is held firmly in its holder and when the weight is symmetrically distributed.

The heated surface was cut on a precision lathe for flatness. It was given a mirror finish to insure that surface roughness was less than film thickness. No attempt was made to make the surface optically flat because of expected thermal distortion during experimental runs.

In the experimental work, it was observed that a loosely held sample of dry ice emits a constant tone that is reminiscent of the familiar sound produced by the vibrations of a coin placed on a piece of dry ice. When such vibrations occur, the steady state analysis of this paper is not applicable. Fortunately it was found that no sound was produced when the sample was carefully centered and firmly held in its holder.

The experimental data required to determine T_1 and m for a single run (thus M and E for a series of runs) are found from Eqs. (40) and (23). Necessary measurements are T_0, p_∞, q_0, b, W, and $(T_\infty)_{sol}$. Values of viscosity, thermal conductivity, and the enthalpies associated with evaporation are also necessary. For all runs, the enthalpy difference between actual and solid-gas equilibrium temperatures is negligible compared to the enthalpy of evaporation.

Values of measured and calculated quantities for a typical experimental run are as follows:

Measured quantities

$T_0 = 311.0$ °K $\quad p_\infty = 0.99$ atm

$q_0 = 0.877$ cal/cm² sec $\quad b = 2.22$ cm

$W = 1090$ g $\quad \mathcal{W} = W/\pi b^2 p_\infty = 6.85\ (10)^{-2}$

Calculated quantities

$T_1 = 224.4$ °K $\quad m = 5.80\ (10)^{-3}$ g/cm² sec

$z_1 = 3.48\ (10)^{-3}$ cm $\quad u_{max} = 1.46\ (10)^3$ cm/sec

The results of the experiments are consistent with the assumptions of the theory and of the experimental apparatus design. The film thickness is over 600 times the length of the mean free path (calculated by the hard sphere model of kinetic theory for mean film temperature) for the typical run. The continuum model is therefore justified. The speed of sound at mean film temperature is over 17 times the maximum velocity, so that compressibility effects are indeed negligible in the gas film. The wavelengths of visible light vary from $4(10)^{-5}$ to $7(10)^{-5}$ cm. The local surface roughness of a mirror finish surface is less than a quarter wavelength of visible light. The heated surface roughness is therefore small compared to the film thickness. The Reynolds number, relating inertia force to viscous force is

$$Re = \frac{\rho u(\partial u/\partial r)}{\mu(\partial^2 u/\partial z^2)} \leq \frac{3}{32}\frac{mz_1}{\mu} = 0.0142$$

which is small as was assumed. The Arrhenius formula for the evaporation of a solid is strictly correct for a one-way reaction in vacuo. It is approximately correct when the ratio $[(p_{eq} - p)/p_{eq}]$ is nearly unity.[9] p_{eq} is the solid-gas equilibrium pressure at evaporating surface temperature. Since the calculated evaporating surface temperatures are greater than the triple point temperature, appropriate values of p_{eq} are found by extrapolation of the Clausius-Clapeyron relation. For the dry ice experimental runs, $0.84 \leq [(p_{eq} - p_{av})/p_{eq}] \leq 0.91$.

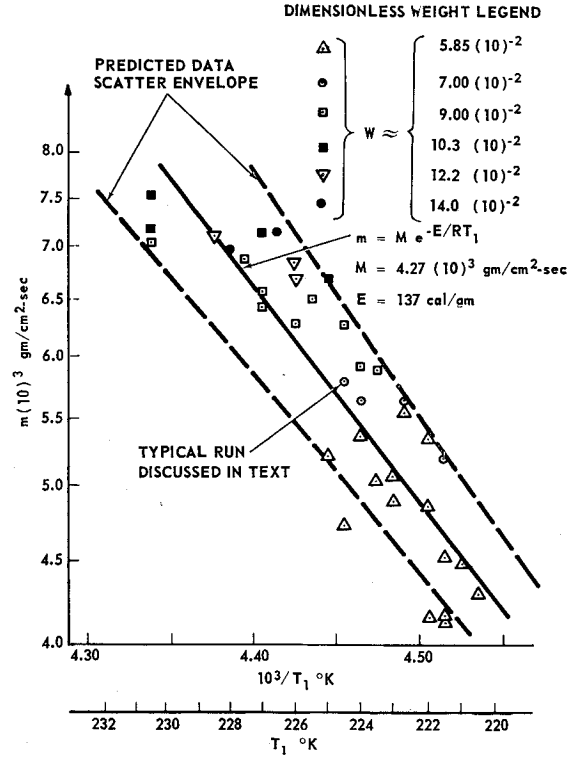

Fig. 9 Mass flux vs calculated evaporating surface temperature for commercial grade dry ice

Locations of the evaporating surface temperatures and average film pressures are compared to the extrapolated solid-gas equilibrium curve in Fig. 8.

Mass flux vs evaporating surface temperature is plotted in Fig. 9 for 37 experimental runs. The points are scattered about the curve $m = M \exp(-E/RT_1)$ where $M = 4.27(10)^3$ g/cm²-sec and $E = 137$ cal/g. The slope of the curve is chosen so that $E = L_s$ in accordance with the theories for evaporation rates.

The scatter of the data in Fig. 10 is not believed unreasonable. An estimate of expected scatter is made by determining the effects of error in T_0, q_0, and b on the calculated values of T_1 and m. It is assumed that no error was made in determining p_∞ and W. Two measurements of temperature and heat flux were taken at least 30 sec apart. If either temperature reading differed from the average by more than 1 °K or if either heat flux differed from the average by more than 1%, the run was rejected on the basis that steady state conditions did not prevail. Measurement of b is believed accurate within ±0.05 cm.

A root mean square error analysis for T_1 and m based on the maximum error in T_0, q_0, and b has been used to determine the expected data scatter curve in Fig. 10. The rms error is not an expected statistical standard deviation because the magnitude of error in each quantity is the maximum allowed and is not based on a statistical average. The use of maximum expected experimental error in the error analysis should roughly compensate for not estimating round-off error in the numerous calculations and for any scatter due to chemical variations in the specimens for the various runs.

A comparison of the present and previous interpretations of pyrolysis data is given in Figs. 9 and 10. Figure 9 shows the experimental data where gas film effects have been considered. Figure 10 shows the calculated evaporation rate vs heated surface temperature. The latter plot completely neglects gas-film effects. Neglect of gas-film effects does not give the expected activation energy, shows that the data obtained depend on the dimensionless weight, and shows a larger data scatter; the larger data scatter is not immediately evident because of the different temperature scales of the two graphs. Anderson et al.[3] report that the results of pyrolysis experiments are independent of weight loading and ambient pressure (effectively dimensionless weight). These are definitely not the findings of this study. It is interesting

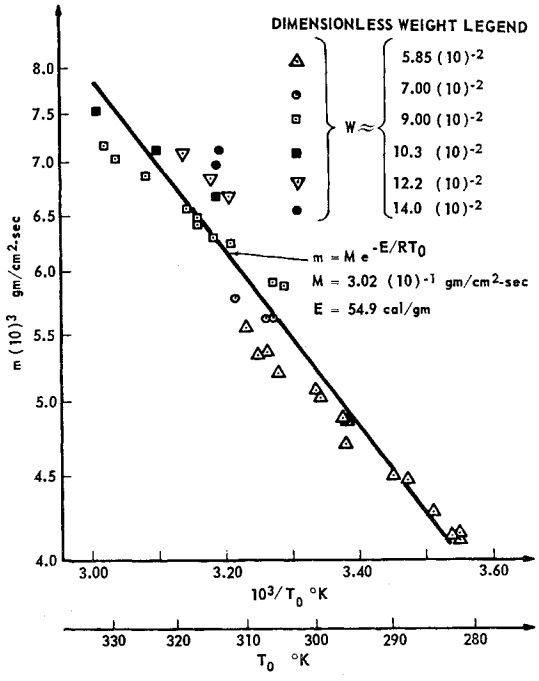

Fig. 10 Mass flux vs heated surface temperature for commercial grade dry ice

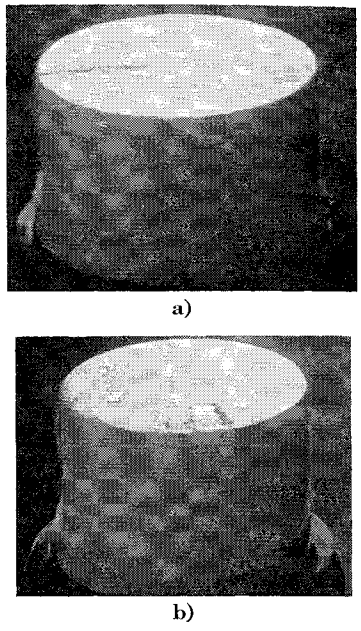

Fig. 11 Dry ice surfaces exhibiting channeling phenomenon

a)

b)

to speculate that their observation is somehow connected with the channeling phenomenon discussed in the following paragraph.

It would be desirable to have data for larger and smaller values of the evaporation rate. Larger evaporation rates were observed, but they could not be interpreted by the theory because well-defined channels formed in the surface of the specimens. (See Fig. 11.) The smooth surface approximation is not valid when channels form. Attempts to observe smaller rates were unsuccessful because of ice formation on the heated surface. The dry ice probably contained a trace of water as a chemical impurity.

Conclusions

The principal conclusion of this study is that gas-film effects can be significant in the linear pyrolysis of solids. The gas-film theory is believed to be quantitatively accurate because it is based on well-established physical principles, because the assumptions of the theory are consistent with the calculated results, and because the data confirm the theoretical activation energy.

The work on dry ice could be extended to include faster and slower rates of evaporation. This would require chemically pure dry ice. However, the trends established by the present work are believed sufficiently clear. Instead of doing more work on dry ice pyrolysis, the extension of the theory to include the additional difficulties of gas-film chemical reactions, diffusion of species, and perhaps a different range of parameters would be of much greater use to workers in the solid propellant field.

In a recent paper, Nachbar and Williams[10] propose that a porous heated plate be used in future linear pyrolysis experiments. They develop a theory to include gas-film reaction and diffusion in a one-dimensional flow field. The one-dimensional analysis has definite theoretical advantages over a possible extension of the present work. However, the additional experimental problem of film thickness measurement is introduced in their proposal. No matter what course is taken in future work, Nachbar and Williams and the author agree that gas-film effects must be considered.

References

[1] Wilfong, R., Penner, S. S., and Daniels, F., "An hypothesis for propellant burning," J. Phys. Colloid Chem. 54, 863–872 (1950).

[2] Barsh, M. K., Andersen, W. H., Bills, K. W., Moe, G., and

Shultz, R. D., "Improved instrument for the measurement of linear pyrolysis rates of solids," Rev. Sci. Instr. **29**, 392–395 (1958).

[3] Andersen, W. H., Bills, K. W., Dekker, A. O., Mishuck, E., Moe, G., and Shultz, R. D., "The gasification of solid ammonium nitrate," Jet Propulsion **28**, 831–832 (1958).

[4] Schultz, R. D. and Dekker, A. O., "Absolute thermal decomposition rates of solids. Part II. The vacuum sublimation rate of molecular crystals," J. Chem. Phys. **23**, 2133–2138 (1955).

[5] Barrere, M., Jaumotte, A., deVeubeke, B. F., and Vandenkerckhove, J., *Rocket Propulsion* (Elsevier Publishing Co., Amsterdam, 1960), p. 228.

[6] Cantrell, R. H., Jr., "Gas film effects in the linear pyrolysis of solids," Ph.D. Thesis, Harvard Univ., Cambridge, Mass. (May 1961).

[7] Schlichting, H., *Boundary Layer Theory* (Pergamon Press, New York, 1955), pp. 87–90.

[8] Hilsenrath, J., "Tables of thermal properties of gases," Natl. Bur. Standards Circular 564 U. S. Government Printing Office, Washington, D. C. (1955).

[9] Knacke, O. and Stranski, I. N., "The mechanism of evaporation," Progr. Metal Phys. **6**, 181–235 (1956).

[10] Nachbar, W. and Williams, F. A., "On the analysis of linear pyrolysis experiments," *Ninth Symposium (International) on Combustion* (Academic Press, New York, 1963), pp. 345–357.

JULY 1963 AIAA JOURNAL VOL. 1, NO. 7

Scale Effects and Correlations in Nonequilibrium Convective Heat Transfer

DANIEL E. ROSNER*
AeroChem Research Laboratories, Princeton, N. J.

The effect of chemical nonequilibrium on the dependence of heat flux on physical scale is illustrated for the case of simultaneous gas-phase and surface-catalyzed-atom recombination. Altitude-velocity regimes in which one can expect appreciable chemical nonequilibrium effects on the heat flux and its scale dependence are displayed and combined with trajectory information for representative hypersonic vehicles. Approximate but rather general correlation equations are suggested for the nonequilibrium boundary-layer regime.

Nomenclature

c_p = specific heat of mixture
D_{12} = atom-molecular binary diffusion coefficient
G = $(\delta^2/D_{12})/\tau$, gas-phase recombination rate parameter
H = $r_D \cdot \Delta h_{\text{chem, eq}}/\Delta h_f$
h = altitude
k_R = termolecular, homogeneous atom recombination rate constant
k_w = first-order rate constant for heterogeneous atom recombination[8, 28]
Le_f = Lewis number $\equiv D_{12}/[\lambda_f/(\rho c_{p,f})]$
m = exponent in the power-law relation $\dot{q}'' \propto \delta^m$, Eq. (4)
n = total number density or $4 + d \ln \epsilon_w / d \ln T_w$
Nu = $\dot{q}''/[\lambda_f(T_e - T_w)/\delta]$
p = local pressure
Pr_λ = Prandtl number for heat conduction = $(\mu/\rho)/[\lambda/(\rho c_p)]$
Pr_D = Prandtl number for diffusion = $(\mu/\rho)/D_{12}$
$\dot{q}''$ = energy transfer rate per unit area of solid
r_D = recovery factor for chemical energy [Le_f for conductivity cell, $(Le_f)^{0.6}$ for stagnation point boundary layer]
R_B = nose radius of body
St_D = local Stanton number for atom transport
T = absolute temperature
u = component of gas velocity parallel to surface
V_∞ = velocity of vehicle with respect to undisturbed atmosphere
W = $k_w\delta/D_{12}$ = catalytic parameter
α = mass fraction of atoms
β = inviscid velocity gradient at nose
γ = recombination coefficient
δ = plate spacing or boundary-layer thickness
ϵ_w = total hemispheric emittance
λ = thermal conductivity of mixture
μ = dynamic viscosity of mixture
ν = kinematic viscosity of mixture; μ/ρ
ξ = $[G(1 + H)]^{1/2}$
ρ = mass density of mixture
σ = Stefan-Boltzmann radiation constant
τ = recombination relaxation time[25] in gas phase
ϕ = extent of recombination = $(\alpha_e - \alpha_w)/\alpha_e$ $(= \Delta h_{\text{chem}}/\Delta h_{\text{chem, eq}})$
Δ = operator meaning change in (across conductivity cell or boundary layer)
$0(\ )$ = order of magnitude symbol

Subscripts

chem = chemical contribution
D = pertaining to atom-molecule diffusion
e = at hot boundary or outer edge of boundary layer
eq = pertaining to local thermochemical equilibrium
f = chemically "frozen," i.e. excluding thermochemical contribution
G = at constant G
W = at constant W
w = at wall (gas/solid interface)
λ = pertaining to molecular conduction
1 = atoms
2 = molecules
∞ = relative to upstream infinity (undisturbed atmosphere)

Received by ARS December 5, 1962; revision received May 28, 1963. This paper is a revised and expanded version of Ref. 1. This research was carried out under Contract AF 49(638)-1138 with the Propulsion Division of the Office of AeroSpace Research, Air Force Office of Scientific Research. It is a pleasure to acknowledge the assistance of F. Kuehner and the computation center of Pfaudler Permutit Inc. (under the direction of J. Cosier) in providing IBM 1620 solutions to the conductivity cell problem. The suggestions of S. Bogdonoff and financial support of the Propulsion Division of the Office of Aerospace Research, Air Force Office of Scientific Research (J. Masi, Chief) also are acknowledged gratefully. For providing the groundwork that made this brief study possible, the author is especially indebted to the many authors whose work is implicitly or explicitly represented in the references.

* Aeronautical Research Scientist. Member AIAA.